Proceedings of the ASME 2019 38th International Conference on Ocean, Offshore and Arctic Engineering
OMAE2019
June 9–14, 2019, Glasgow, Scotland, UK

OMAE2019-95093

A SEMI-ANALYTICAL METHOD FOR CALCULATING THE HYDRODYNAMIC FORCE ON PERFORATED PLATES IN OSCILLATING FLOW

Fredrik Mentzoni* **and Trygve Kristiansen**

Department of Marine Technology
Norwegian University of Science and Technology
NO-7491 Trondheim, Norway

ABSTRACT

A two-dimensional numerical analysis on the hydrodynamic force of perforated plates in oscillating flow is presented, and a new semi-analytical force model is proposed. Plates with ten different perforation ratios, τ, from 0.05 to 0.50 are simulated. The Keulegan–Carpenter numbers in the simulations cover a range from 0.002 to 2.2 when made nondimensional with the width of the plates. Resulting hydrodynamic added mass and damping coefficients are presented. All perforated plates with perforation ratios greater than or equal to 10 % are found to be damping dominant. The numerical results are obtained using a two-dimensional Navier–Stokes solver (CFD), previously validated against dedicated 2D experiments on perforated plates. Furthermore, we present verification of the code against the analytical solid flat plate results by Graham. The presently obtained hydrodynamic coefficients are compared with the state-of-the-art semi-analytical method for force coefficient calculation of perforated plates by Molin, as well as the recommended practice for estimating hydrodynamic coefficients of perforated structures by DNV GL. Based on the CFD results, a new method for calculating the hydrodynamic force on perforated plates in oscillating flow is presented. The method is based on curve fitting the present CFD results for perforated plates, to the analytical expressions obtained for solid plates by Graham. In addition to its simplicity, a strength of the method is that coefficients for both the added mass and damping are obtained.

*Corresponding author: fredrik.mentzoni@ntnu.no

INTRODUCTION

Perforated and ventilated structures are commonly found in many marine applications. Examples include heave plates, wave absorbers, damping plates, hatch covers, mudmats and various protection equipments used on complex subsea structures. Many of these structures have large widths and lengths compared to their thickness, and can, in terms of flow and resulting loads, be simplified as perforated plates. Due to the industrial relevance, there has been a great deal of analytical, numerical and experimental investigations on perforated plates. Molin [1] presented an extensive review in 2011. A brief summary of some other relevant studies performed after 2011 is given in [2].

The present study is part of a bigger project (MOVE), where the motivation is to reduce uncertainty when performing marine deployment operations, which is likely to be cost saving by reducing conservatism and delays when it comes to the time used on waiting for acceptable weather conditions. The hydrodynamic behavior and forces on perforated plates are relevant in this respect. One objective of the project involves increased knowledge on the hydrodynamic loads on typical members of subsea structures, including how to account for interaction and shielding effects between different member types. In an initial study, experimentally obtained hydrodynamic force coefficients for different configurations of perforated plates and cylinders were presented [3]. The hydrodynamic forces on perforated plates is identified as the most important contribution to the total force on a subsea module. Challenges with estimating the hydrodynamic coefficients from experiments were highlighted. The initial study

was followed up with further experimental investigations and the development of a numerical viscous flow solver which can estimate hydrodynamic coefficients of subsea structures in a two-dimensional setting [2]. Special attention was given to the effect of flow separation at the ends of perforated plates, which has been pointed out by several previous studies to be of importance [1, 4–7].

In the current study, we present a numerical analysis on the hydrodynamic forces of perforated plates in oscillating flow. We compare results from our numerical viscous solver with the state-of-the-art method for calculating hydrodynamic coefficients of perforated plates, and focus on how to easily estimate hydrodynamic coefficients of perforated plates. A large range of numerical simulations are performed for perforated plates with perforation ratios, τ, from 0.05 to 0.50, for Keulegan–Carpenter (KC) numbers,

$$\mathrm{KC} = \frac{WT}{D}, \tag{1}$$

of $0.002 \leq \mathrm{KC} \leq 2.2$. Here W is the amplitude of the velocity, T the period of motion and D the plate width. The present range of KC numbers covers typical KC numbers for perforated plate structures used in marine operations.

The structure of the present text is explained in the following. First, the numerical method (CFD) is presented. Details on the discretization of the perforated plates are given in this section. We briefly describe the results from the validation of the CFD against dedicated 2D perforated plate experiments. Furthermore, a presentation of our CFD results from simulations of solid plates are presented, and compared against the analytical investigation by Graham [8]. Next, we summarize the semi-analytical method by Molin [9, 10]. A summary of the recommendations for calculating hydrodynamic coefficients on perforated structures by DNV GL [11] is then given. We next proceed to the CFD results from the present simulations of perforated plates in oscillating flow. Comparisons are given with calculations performed using the semi-analytical method. We end our result section by presenting coefficients found when curve-fitting our CFD results for perforated plates, to the analytical expressions obtained by Graham for solid plates, thereby proposing a new semi-analytical force model for perforated plates. Finally, conclusions are drawn in the last section.

NUMERICAL METHOD

A two-dimensional Navier–Stokes solver, based on the fractional-step method, as that by Chorin [12], is used in the present analysis. The abbreviation CFD (computational fluid dynamics) refers to this solver and its results throughout the paper. A staggered grid is used in the solver, where the grid cells are geometrically stretched from a fine region close to the perforated plates, towards larger cells closer to the boundaries of the computational domain. The boundaries in the computational domain are placed far from the plates (total domain size, l, is $6\,\mathrm{m} \times 6\,\mathrm{m}$ corresponding to $\frac{l}{D} = 14.3$-16.7, cf. Table 1), such that the simulations represent infinite fluid conditions.

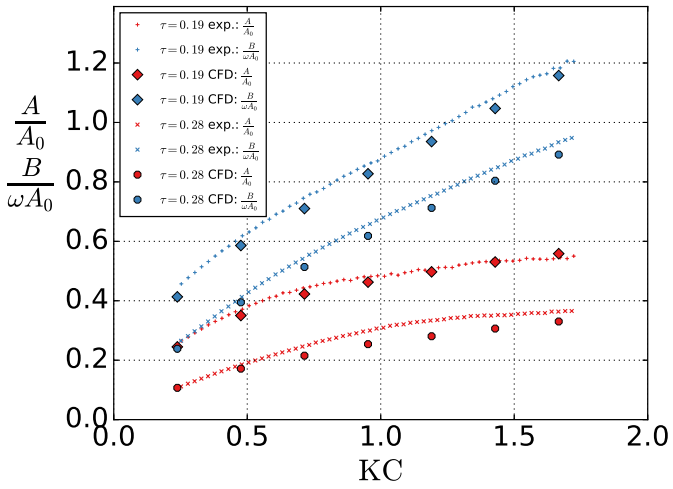

FIGURE 1. VALIDATION OF PRESENT NUMERICAL METHOD AGAINST EXPERIMENTAL DATA OF PERFORATED PLATES. DETAILS PROVIDED IN [2].

TABLE 1. DESCRIPTIVE PARAMETERS OF THE DISCRETIZATION OF PLATE MODELS I AND II. PLATE WIDTH (D), WIDTH-TO-THICKNESS ($\frac{D}{t}$), WIDTH-TO-HOLE-SIZE ($\frac{D}{l_h}$), WIDTH-TO-CELL SIZE IN THE FINE GRID REGION CLOSE TO THE PLATE ($\frac{D}{\Delta}$), DOMAIN SIZE TO PLATE WIDTH ($\frac{l}{D}$), AND TOTAL NUMBER OF GRID CELLS IN THE DOMAIN.

Model	D	$\frac{D}{t}$	$\frac{D}{l_h}$	$\frac{D}{\Delta}$	$\frac{l}{D}$	Cell count
I	0.42 m	140	140	280	14.3	74 268
II	0.36 m	120	80	240	16.7	67 860

The numerical solver has previously been validated against dedicated 2D experiments on perforated plates [2]. Selected results from the validation are presented in Fig. 1. Experimentally obtained hydrodynamic coefficients for two perforated plates, with perforation ratios of 19 % and 28 %, are here compared to simulation results of numerically modeled perforated plates with corresponding perforation ratios by the presented CFD. The experiments were conducted in a wave flume at the Marine Technology Center in Trondheim, well suited for performing forced oscillation tests of perforated plates. A considerable amount of

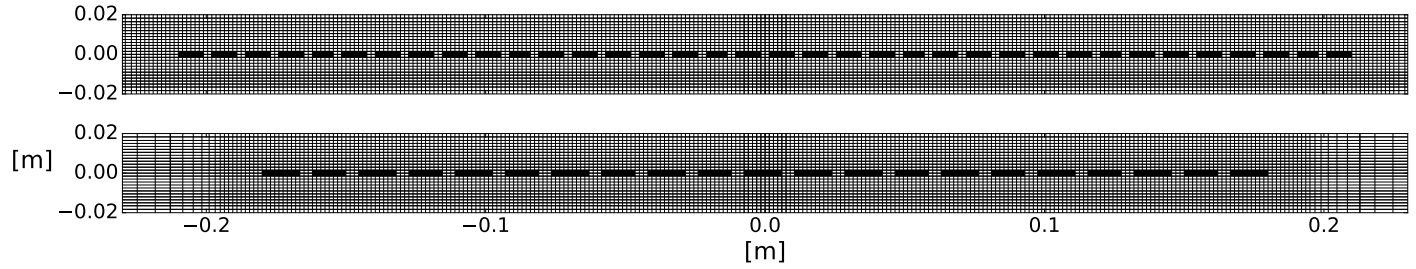

FIGURE 2. ILLUSTRATIONS OF THE FINE REGION OF THE CFD GRIDS FOR PLATES WITH PERFORATION RATIO $\tau = 0.25$ USING PLATE MODELS I (TOP) AND II (BOTTOM). TOTAL DOMAIN SIZE IS $6\,\mathrm{m} \times 6\,\mathrm{m}$.

work was invested to ensure the general quality of the experiments. In addition to force and motion measurements, the free-surface elevation was measured during the tests, and the corresponding wave-radiation damping found to be unimportant. The vertical motions of the oscillating plates were monitored by several accelerometers. Special care was taken to ensure an instrumental setup where the measured force and accelerations have zero phase delay, in order to obtain reliable hydrodynamic force coefficients. For a more thorough description of the experimental setup, we refer to previous studies [2, 3].

In the experimental investigations used to validate the CFD, perforated plates were forced to oscillate in otherwise still water. In the CFD, on the other hand, the plates are fixed while prescribed oscillating flow conditions are set as boundary conditions on the computational domain boundaries, such that the plates experience an ambient, sinusoidally oscillating flow. Since the fluid is oscillating in the CFD, the total calculated force on the plates consists of the hydrodynamic diffraction force and the Froude–Krylov force. In order to have comparable results between the experiments and CFD, the Froude–Krylov force is subtracted in the CFD. Further, the diffraction force is decomposed in a damping term, proportional to the prescribed velocity, and an added mass term, proportional to the acceleration,

$$A\ddot{\eta} + B\dot{\eta} = F_H, \tag{2}$$

with A being the added mass coefficient, $\ddot{\eta}$ the acceleration of the ambient flow, B the damping coefficient, $\dot{\eta}$ the velocity of the ambient flow, and F_H the hydrodynamic diffraction force. The added mass and damping coefficients are obtained by Fourier averaging,

$$A\int_{mT} \ddot{\eta}\,\ddot{\eta}\;dt + 0 = \int_{mT} F_H\,\ddot{\eta}\;dt, \tag{3}$$

$$0 + B\int_{mT} \dot{\eta}\,\dot{\eta}\;dt = \int_{mT} F_H\,\dot{\eta}\;dt. \tag{4}$$

Here m indicates the oscillation number. The CFD results are based on simulations lasting ten oscillation periods. The five first oscillation periods are ignored. The measured force on the plates in the last five oscillation periods is then used to calculate the hydrodynamic coefficients, that is, $m = 6, 7, 8, 9, 10$. The mean value from these five oscillation periods are presented in the result figures. The standard deviation between the coefficients from these five m are also calculated, but are found to be small in all cases, in general less than 1 % of the mean value. To increase readability, the standard deviations are not plotted in the result figures. The coefficients are made nondimensional by the analytical added mass of a solid flat plate. In two-dimensional flow, this is

$$A_0 = \frac{\pi}{4}\rho D^2, \tag{5}$$

where ρ is the fluid density. Nondimensional damping coefficients are obtained by dividing B with A_0 times the circular frequency of motion, ω.

A total of ten perforation ratios, ranging from $\tau = 0.05$ to $\tau = 0.50$ are investigated. The perforated plates are discretized using multiple plate elements of solid cells, with openings between them containing fluid cells, cf. Fig. 2. We follow the findings of [2] regarding mesh size and number of holes in the plates; the results converged with seven plate elements and grid cell sizes of $\Delta = 2\,\mathrm{mm}$. Two different numerical perforated plate models, I and II, with different numerical meshes, widths and number of fluid cells in the openings, are tested for each perforation ratio, in order to increase the confidence in the results, and to investigate the numerical uncertainty of different modeling of the same plate perforation. Details of plate models I and II are given in Table 1. The two meshes are illustrated in Fig. 2.

One of the advantages of the numerical viscous flow solver is the ability to easily visualize and observe features of the flow

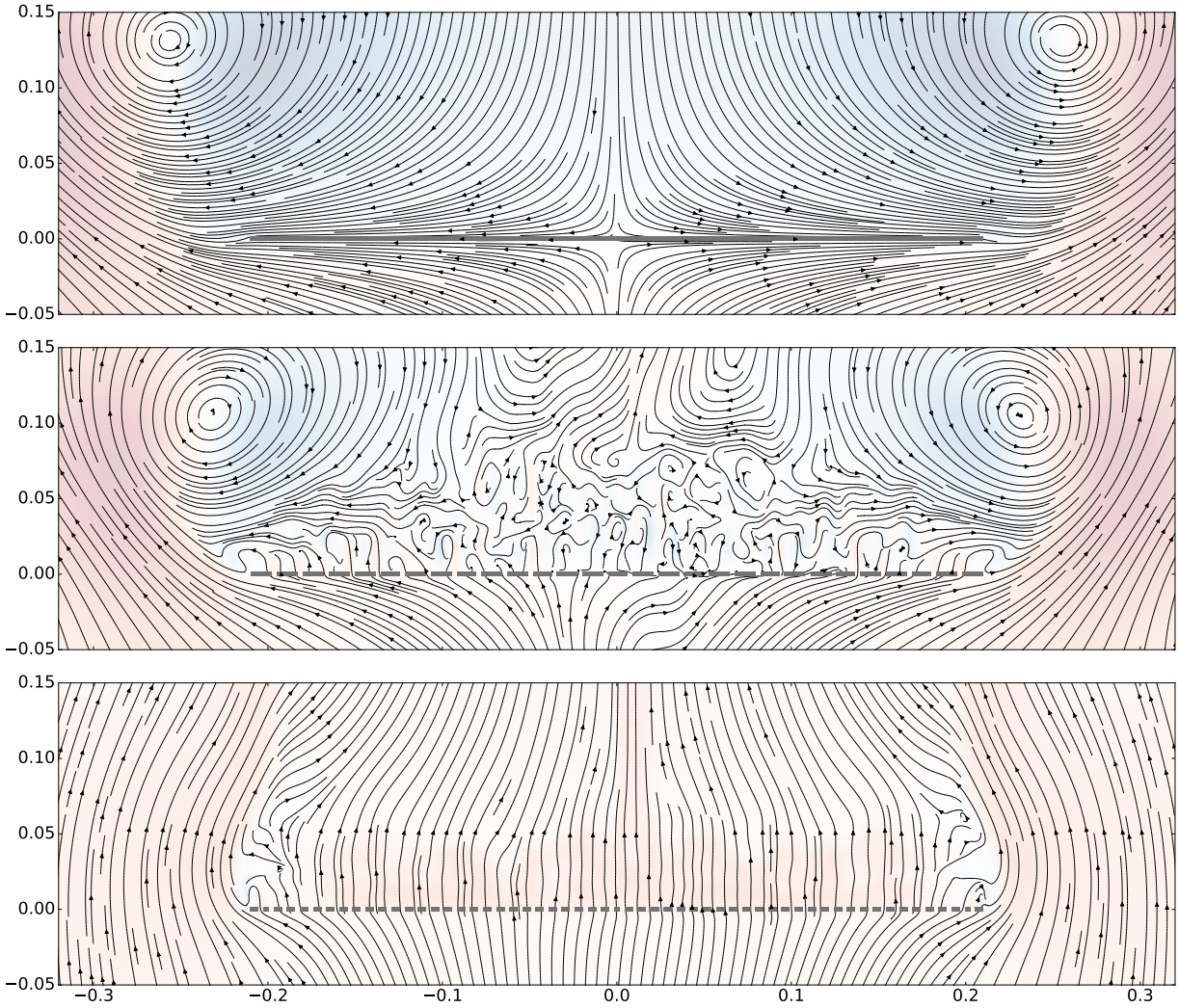

FIGURE 3. STREAMLINES FOR $\tau = 0$ (TOP), $\tau = 0.20$ (MIDDLE) AND $\tau = 0.40$ (BOTTOM) AT KC $= 0.95$. THE PLOTS ARE OBTAINED 41 % INTO AN OSCILLATION PERIOD. RED CONTOURS USED FOR POSITIVE VERTICAL VELOCITY, BLUE FOR NEGATIVE.

field. Examples of flow fields are provided in Fig. 3. Here, streamline plots for simulations with plate model I at KC $= 0.95$ are provided for $\tau = 0$ (top), $\tau = 0.20$ (middle) and $\tau = 0.40$ (bottom). The color map for the contours represent the vertical velocity (red for positive, blue for negative). The plots are zoomed in on the plates at a time-instant 41 % into an oscillation period where the velocity at the boundaries is set to $w = W\sin(\omega t)$. Note that the flow is globally deflected towards the sides of the plate even for high perforation ratios, similar to that for a solid plate. Vortices due to plate-end flow separation is easily observed for $\tau = 0.2$. A closer view reveals vortical structures behind each plate element at the scale of the plate element lengths for all perforation ratios.

GRAHAM'S SOLID PLATE MODEL

We next turn to the analytical results by Graham for solid plates [8]. In his analysis of the hydrodynamic forces on sharp-edged objects at low KC numbers, Graham found that the added mass and damping coefficients of a solid plate were functions of $\mathrm{KC}^{\frac{2}{3}}$,

$$\frac{A}{A_0} = a_0 + a_1 \mathrm{KC}^{\frac{2}{3}}, \tag{6}$$

$$\frac{B}{\omega A_0} = \frac{b_1}{\pi^2} \mathrm{KC}^{\frac{2}{3}}. \tag{7}$$

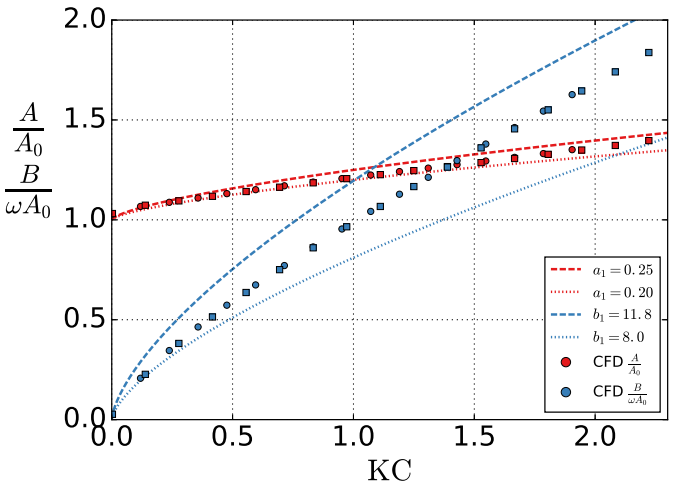

FIGURE 4. ADDED MASS (RED) AND DAMPING (BLUE) COEFFICIENTS OF A SOLID PLATE FROM CFD. CIRCULAR MARKERS: MODEL I. SQUARE MARKERS: MODEL II. COMPARISON WITH THE ANALYSIS BY GRAHAM [8]; THEORETICAL ($a_1 = 0.25, b_1 = 11.8$) AND EXPERIMENTAL FIT ($a_1 = 0.2, b_1 = 8.0$) PRESENTED WITH, RESPECTIVELY, DASHED AND DOTTED LINES.

TABLE 2. CURVE FIT OF PRESENT SOLID PLATE CFD SIMULATIONS TO EQS. (6) AND (7).

Model	a_0	a_1	b_1
I	1.007	0.2137	10.03
II	1.003	0.2179	10.16
Combined	1.005	0.2160	10.11

The theoretical analysis yielded $a_0 = 1$, $a_1 = 0.25$ and $b_1 = 11.8$. Curve-fit with the experimental results in the KC number range $\approx$ 3-7 by Singh [13], gave somewhat smaller values for the coefficients, $a_1 = 0.2$ and $b_1 = 8.0$ [8]. Note that the KC number range for which this was based on, was quite modest.

The resulting coefficients from the solid plate validation case of the present CFD are compared to the analytical results by Graham and presented in Fig. 4. As for the perforated plates, two solid plate models are simulated with the present CFD, denoted I and II, in a similar manner as that of the perforated plates. Only minor differences are found between plate models I and II. Due to the finite thickness of the numerically simulated plates, the low-KC limit added mass is slightly larger than the theoretical value of 1 for an ideal flat plate (zero thickness). The numerical simulations yield coefficients that are, in general, between the theoretically and experimentally obtained a_1 and b_1. Resulting a_0, a_1 and b_1 based on curve fit of the numerical simulations are provided in Table 2.

We return to Graham's model in the last section of our paper.

MOLIN'S SEMI-ANALYTICAL METHOD

Assuming a quadratic pressure-drop condition for the flow through the openings of a perforated object, combined with the assumption of potential flow conditions in the fluid domain, such that all vorticity is constrained to a thin strip coinciding with the plate, Molin developed a method for estimating hydrodynamic coefficients of perforated structures [9, 10]. A notable finding of the method is that both the added mass and damping coefficients are functions of the amplitude of motion. Furthermore, both coefficients have the limiting value of zero when the amplitude goes to zero.

For the case of an oscillating two-dimensional perforated plate, the hydrodynamic coefficients can be obtained from Fourier-series by eigenfunction expansion of the velocity potential [1], or, as shown in An and Faltinsen [14], by assuming anti-symmetric vortices distributed along the plate. The resulting hydrodynamic added mass and damping coefficients are found to be functions only of the so-called perforated KC number,

$$\mathrm{KC}_{por} = \frac{Z}{D}\frac{(1-\tau)}{2\mu\tau^2}. \tag{8}$$

Hence, the force coefficients are functions of the amplitude of motion, Z, the width of the plate, D, the perforation ratio, τ, and the discharge coefficient, μ, only. The discharge coefficient is a function of the local geometry of the plate openings.

The original semi-analytical method does not take flow separation at the plate-ends into account. Flow separation at the plate-ends will in general increase the damping and reduce the added mass coefficient [6]. In order to account for the plate-end flow separation effect, Sandvik et al. [5] proposed to add a drag force term, which in 2D is written

$$F = \frac{1}{2}\rho C_D D \overline{w}_r |\overline{w}_r|, \tag{9}$$

with a drag coefficient inspired by the solid flat plate analytical investigation by Graham [8],

$$C_D = \alpha \mathrm{KC}^{-\frac{1}{3}}. \tag{10}$$

The relative velocity in the drag force term, $\overline{w}_r$, is the plate velocity minus the relative fluid velocity through the plate, averaged over the plate [1]. Consequently, with the drag force term added,

both the added mass and damping coefficients become functions of KC in addition to KC_{por}. The semi-analytical method including the drag correction term represents the state-of-the-art for force coefficient calculation of perforated plates. Later in the text, we compare the method with the results from our CFD.

In the semi-analytical method, the drag correction coefficient, α, and discharge coefficient, μ, must be determined. When compared with the solid plate results by Graham, α of Eq. (10) corresponds to b_1 of Eq. (7). Graham's theoretical analysis yielded $b_1 = \alpha = 11.8$. For a perforated plate, the flow separation at the plate ends will be weaker than for a solid plate [4, 6], and consequently $\alpha < 11.8$. In the present study, a large range of calculations are performed, using 24 different values for α ranging from $\alpha = 0.5$ to $\alpha = 12.0$, with increments of 0.5.

According to Molin et al. [1,6,15], the discharge coefficient is usually $0.3 < \mu < 1.0$. A sensitivity study performed by An and Faltinsen [4], showed that the value of the discharge coefficient is of importance, especially for the added mass coefficient. In his 2011 review [1], Molin presents a number of methods for estimating the loss coefficient, K, where the relation between the loss coefficient and the discharge coefficient is

$$\mu = \frac{1-\tau}{K\tau^2}. \tag{11}$$

For a perforated plate where the perforations have square edges, the loss coefficients provided by Blevins [16, pp. 314–315], corresponds to discharge coefficients in the range $0.35 < \mu < 0.65$ for the presently simulated perforation ratios. Based on this, the present calculations are performed using a range of discharge coefficients from $\mu = 0.3$ to $\mu = 1.0$ with increments of 0.05.

Taking into account the ten different perforation ratios, the 24 values of α and the 15 discharge coefficients, a total of 3600 semi-analytical calculations are performed. For each perforation ratio, the combination of α and μ that corresponds to the smallest mean relative difference between the semi-analytical method and the CFD, for the considered KC numbers, is presented. Three results are provided for each plate perforation, the combination of μ and α that yields the smallest relative difference for 1) the added mass coefficient, 2) the damping coefficient, and 3) both coefficients combined.

DNV GL RECOMMENDED PRACTICE

DNV GL has developed a recommended practice (RP) for modeling and analysis of marine operations, the DNVGL-RP-N103 [11]. Included in the RP are relations for estimating the added mass of perforated structures. As stated in the RP, the added mass of an object in the limit of zero amplitude can be calculated numerically with potential flow assumptions using a source method. Based on results from perforated plates with circular holes, DNV GL provides the following relation for estimating the added mass in the low-KC limit [11, Section 3.3.4].

TABLE 3. LOW-KC LIMIT ADDED MASS OF A PLATE WITH PERFORATION RATIO $\tau = 0.3$ MODELED WITH DIFFERENT NUMBER OF HOLES, n_h, AND CORRESPONDING HOLE SIZE, l_h, TO PLATE WIDTHS, D, USING A SOURCE METHOD.

n_h	$\frac{l_h}{D}$	$\frac{A}{A_0}$	Rel. diff. to (12)
1	0.3	0.284	17 %
2	0.15	0.207	40 %
4	0.075	0.144	58 %
8	0.0375	0.098	71 %
16	0.01875	0.071	79 %
32	0.009375	0.055	84 %
DNV GL		0.343	

$$\frac{A}{A_0} = \exp\left(\frac{-\tau}{0.28}\right). \tag{12}$$

Contrary to the semi-analytical method presented in the previous section, Eq. (12) suggests that perforated plates have a considerable added mass in the low-KC limit. Note that the relation is a function of the perforation ratio only. However, in the low-KC limit, the hole size relative to the plate size is the important parameter for the added mass of a perforated plate. An example is given in Table 3, where the added mass coefficients for plates with a perforation ratio of $\tau = 0.3$, modeled with different hole sizes, are presented. The results are obtained using a numerical source method. The plate thickness is set to 1 % of the plate width, that is $\frac{t}{D} = 0.01$. As illustrated, decreasing the hole size, and thereby increasing the number of holes on the plate, reduces the added mass of the plate. In the semi-analytical method presented in the previous section, the assumption of an infinite number of holes is applied, and the low-KC added mass is zero. In order to get a correct estimate of the low-KC added mass of a specific perforated structure, the number of holes is important.

A relation for the added mass at any KC number is also provided by DNV GL [11, Section 4.6.4],

$$\frac{A}{A_0} = \begin{cases} 1, & \tau \leq 0.05 \\ 0.7 + 0.3\cos\left(\pi\left(\frac{\tau-0.05}{0.34}\right)\right), & 0.05 < \tau < 0.34 \\ \exp\left(\frac{0.1-\tau}{0.28}\right), & 0.34 \leq \tau \leq 0.50. \end{cases} \tag{13}$$

The relation is based on model test data and includes a safety margin. As for the low-KC relation in (12), the all-KC relation in

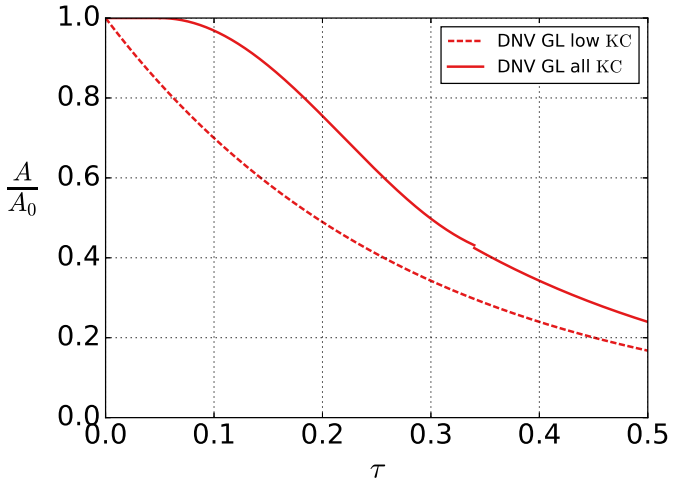

FIGURE 5. ADDED MASS RELATIONS FOR PERFORATED STRUCTURES IN DNVGL-RP-N103, EQS. (12) AND (13) [11].

(13) is a function of perforation ratio only. However, as pointed out in several previous studies, the hydrodynamic coefficients of perforated plates are highly amplitude dependent.

Sections 3.3.4 and 4.6.4 of the RP, titled *Added mass and damping for ventilated structures* and *Effect of perforation*, respectively, contain relations for the added mass coefficients, but no information on how to account for the perforation ratio when estimating damping coefficients. From (2) and (5), the amplitude of the hydrodynamic force can be written as a function proportional to the nondimensional added mass and damping coefficients,

$$\overline{F}_H \propto \sqrt{\left(\frac{A}{A_0}\right)^2 + \left(\frac{B}{\omega A_0}\right)^2}. \tag{14}$$

An increase in the nondimensional added mass coefficient or damping coefficient increases the hydrodynamic force amplitude. Further, the hydrodynamic force amplitude is proportional to the square root of the coefficients squared. Therefore, the larger term dominates, and if for instance $\frac{B}{\omega A} = 2$, damping alone is 89 % of the hydrodynamic force amplitude. Recent investigations have shown that the hydrodynamic force on perforated plates is in general damping dominant, for $\tau \gtrsim 0.1$ [2–6]. A similar outcome is expected for the wave excitation forces. Consequently, proper calculation of the damping coefficient is at least as important as the added mass coefficient.

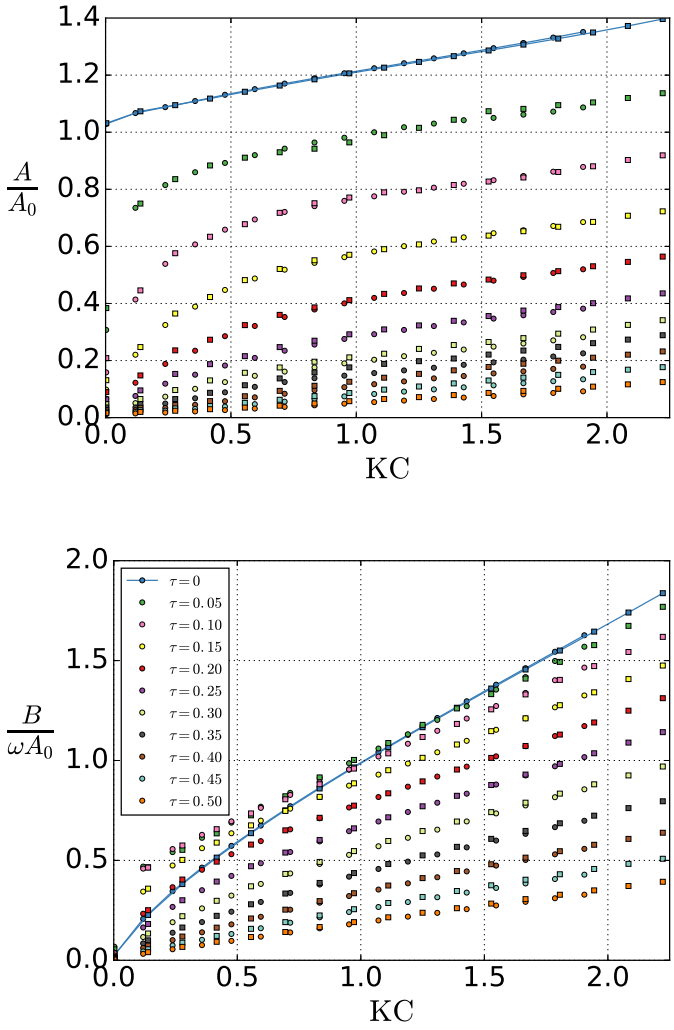

FIGURE 6. ADDED MASS (TOP) AND DAMPING (BOTTOM) COEFFICIENTS FOR NUMERICALLY SIMULATED PERFORATED PLATES. CIRCULAR MARKERS: MODEL I. SQUARE MARKERS: MODEL II.

RESULTS

Added mass and damping coefficients predicted by the present CFD are presented in Fig. 6. As for the solid plate models, there are small differences between the perforated plate models I and II. The added mass clearly increases with decreasing perforation ratio. The largest rate of absolute changes in A appear for $\tau \lesssim 0.20$. For the damping, B, there is a more steady rate of absolute change with decreasing perforation ratio. Notably, P05, P10, P15 and P20 all yield larger damping coefficients than the solid plate, P00, for a range of low KC numbers.

The ratio between the damping force and added mass force

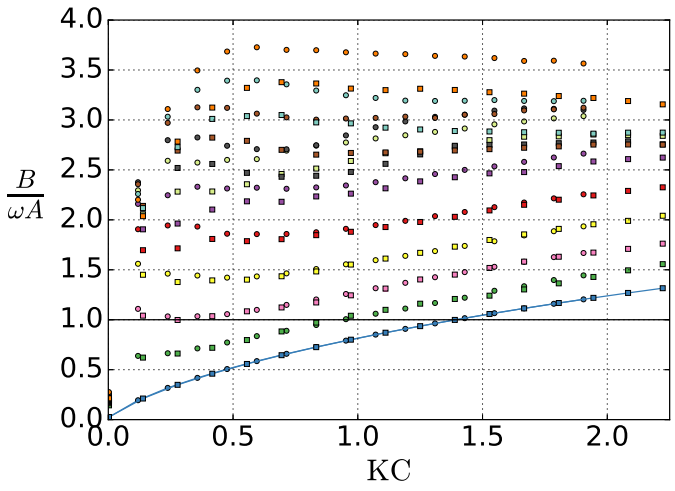

FIGURE 7. RATIO BETWEEN DAMPING FORCE AND ADDED MASS FORCE FOR NUMERICALLY SIMULATED PERFORATED PLATES. LEGEND IN FIG. 6.

is presented in Fig. 7. For practical values of the KC number, perforation ratios larger than $\tau = 0.1$ are found to be damping dominant. Even the densest perforated plate, P05, is damping dominant for KC > 0.95. We would like to stress the importance of this fact.

The results from calculations with Molin's semi-analytical method are presented in Table 4. Three observations are highlighted in the following. 1) Even from a large range of μ and α combinations, the best fit still has a considerable relative difference when compared to the CFD results. The semi-analytical method seems best suited for moderate perforation ratios, and the relative differences are larger for both smaller and larger perforation ratios. 2) There are no generic values of μ and α, and it is not obvious how these parameters should be chosen. The loss coefficients for a perforated plate with square edges provided by Blevins [16, p. 314] suggests that μ should increase from $\mu = 0.35$ for the smallest perforation ratio, $\tau = 0.05$, to $\mu = 0.5$ for the largest perforation ratio, $\tau = 0.5$. However, the present results found the best (combined) fit when μ is larger than 0.5, without much dependency on the perforation ratio. The drag correction coefficient, α, is found to decrease with increasing perforation ratio, ranging from $\alpha = 10.5$ for $\tau = 0.05$ to $\alpha = 1.0$ for $\tau = 0.50$. 3) The best fit to both added mass and damping is in general not found for a single combination of μ and α. Most noticeable is the inconsistent trends in α. For smaller perforation ratios, the best fit to the damping coefficient is found with a larger α than what gives the best fit for the added mass coefficient. This behavior is opposite for higher perforation ratios, that is, for the largest perforation ratios, the added mass best

TABLE 4. THE COMBINATION OF μ AND α THAT YIELDS THE BEST FIT WITH THE ADDED MASS AND DAMPING COEFFICIENTS OF THE CFD RESULTS, SEPARATELY AND COMBINED. MEAN RELATIVE DIFFERENCE ($\overline{d_r}$) AND CORRELATION COEFFICIENT (r) BETWEEN COMBINED SEMI-ANALYTICAL BEST FIT AND CFD RESULTS.

τ	Best $\frac{A}{A_0}$		Best $\frac{B}{\omega A_0}$		Combined best fit			
	μ	α	μ	α	μ	α	$\overline{d_r}$	r
0.05	0.35	0.5	1.0	10.5	1.0	10.5	21 %	0.94
0.10	0.95	2.0	1.0	9.5	0.60	9.5	15 %	0.95
0.15	0.85	4.5	0.95	9.0	0.60	8.0	12 %	0.97
0.20	0.75	5.5	0.85	8.0	0.65	7.0	11 %	0.98
0.25	0.65	6.5	0.80	7.5	0.65	6.5	12 %	0.98
0.30	0.55	7.0	0.80	7.0	0.65	6.0	14 %	0.98
0.35	0.45	7.0	0.75	5.5	0.65	4.5	16 %	0.99
0.40	0.45	6.5	0.75	4.5	0.70	3.0	17 %	0.99
0.45	0.45	5.5	0.75	3.0	0.70	2.0	19 %	0.99
0.50	0.40	6.0	0.80	3.5	0.75	1.0	21 %	0.99

fit is found with a larger α than the damping best fit. A similar problem has previously been observed when comparing the semi-analytical method to experimental results; when comparing the semi-analytical method with experiments of a perforated disk with a perforation ratio of 20 %, Molin et al. [6] found that $\alpha = 6$ was needed to get a good fit for the damping coefficient, but this would underestimate the added mass coefficient. The results by An and Faltinsen [4], comparing the semi-analytical method with experimental results of two rectangular perforated plates of perforation ratios 8 % and 16 %, yielded a similar conclusion.

Of the 3600 different combinations of perforation ratios, discharge coefficients and drag correction coefficients, one of the best fits was found for the 25 % perforation ratio plate using $\mu = 0.65$ and $\alpha = 6.5$. This combination gives a mean relative difference across the considered KC numbers of 12 %. We emphasize, however, that this value of μ is higher than those provided by Blevins. The added mass and damping coefficients predicted by the semi-analytical method for $\tau = 0.25$ and $\mu = 0.65$ for varying α values are presented in Fig. 8. Note, in particular, that the value of α that gives the best fit to the CFD results is depending on the range of KC numbers considered. A similar tendency was found by An and Faltinsen [4].

Added mass and damping coefficients from the CFD simulations, for three KC numbers, are presented as functions of the

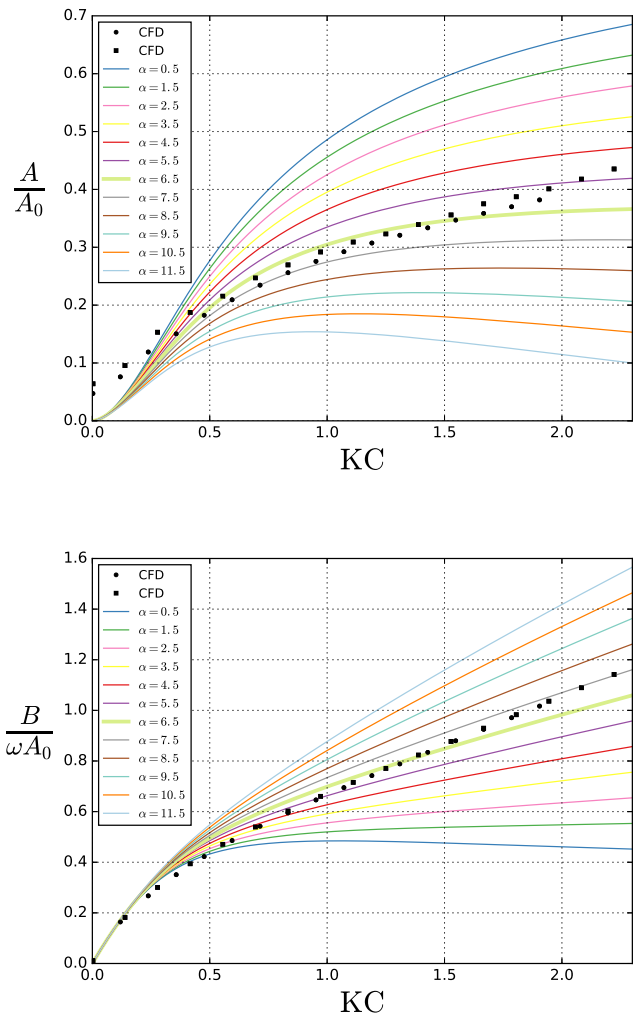

FIGURE 8. ADDED MASS (TOP) AND DAMPING (BOTTOM) COEFFICIENTS FROM MOLIN'S SEMI-ANALYTICAL METHOD FOR $\tau = 0.25$ AND $\mu = 0.65$. EACH CURVE REPRESENTS A GIVEN VALUE OF α. TO INCREASE READABILITY, ONLY 12 OF THE 24 CALCULATED α ARE INCLUDED. MARKERS ARE CFD RESULTS FOR THE PERFORATED PLATE WITH PERFORATION RATIO $\tau = 0.25$.

perforation ratio, τ, in Fig. 9. A similar presentation was given for the added mass relations provided by DNV GL, cf. Fig. 5. Both figures illustrate a reduction of added mass as the perforation ratio increases. However, Fig. 9 highlights the amplitude dependence of the coefficients. Both relations by DNV GL are, in general, conservative compared to the present CFD results, but for small perforation ratios, the relations by DNV GL underestimate the added mass compared to the CFD results. Further, we

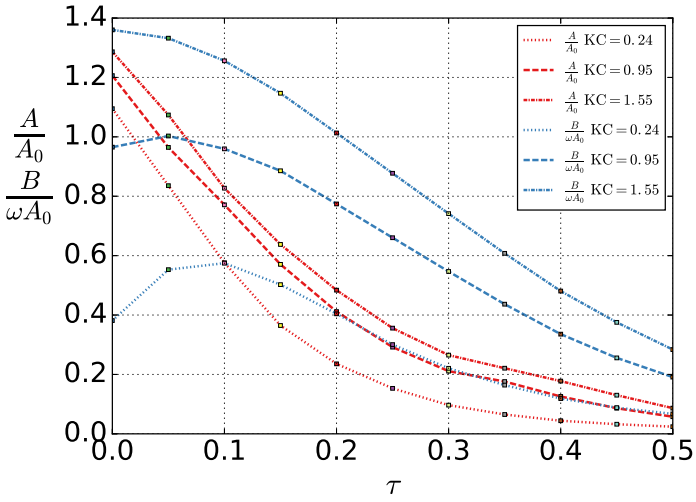

FIGURE 9. ADDED MASS AND DAMPING AS FUNCTIONS OF PERFORATION RATIO AT THREE KC NUMBERS.

emphasize again that the present results highlights the need for including damping, as the damping *force* is in general larger than the added mass force, with increasing relative importance as the perforation ratio increases.

PROPOSED CFD-FITTED SEMI-ANALYTICAL METHOD

Estimating simple relations for the added mass and damping coefficients that are functions of both the KC number and the perforation ratio is, evidently, not trivial. In the following, we propose a semi-analytical model for perforated plates, based on Graham's model for a solid plate [8]. The method is semi-analytical in the sense that it is based on Graham's analytically derived expressions, Eqs. (6) and (7), but with the parameters, a_0, a_1 and b_1, curve-fitted to our present CFD results for perforated plates. Since the present CFD is well validated with experiments for perforated plates, we argue that the model is well rooted in the physics.

For each perforation ratio, the resulting parameters, a_0, a_1 and b_1, are presented in Table 5. Comparisons of the curve-fits to the CFD results are presented in Fig. 10. The applied functional relationship, i.e. Eqs. (6) and (7), seems to provide a reasonable model. A deficiency is that the damping coefficients are underestimated for the densest perforated plates at low KC numbers. Note that the perforated plates in the CFD, and the experimentally investigated perforated plates which the CFD was validated against, have sharp edged openings. This is likely to give conservative coefficients. Sandvik et al. [5] performed an experimental investigation of a realistic hatch cover model (a perforated protection structure for subsea modules), consisting of rows of cir-

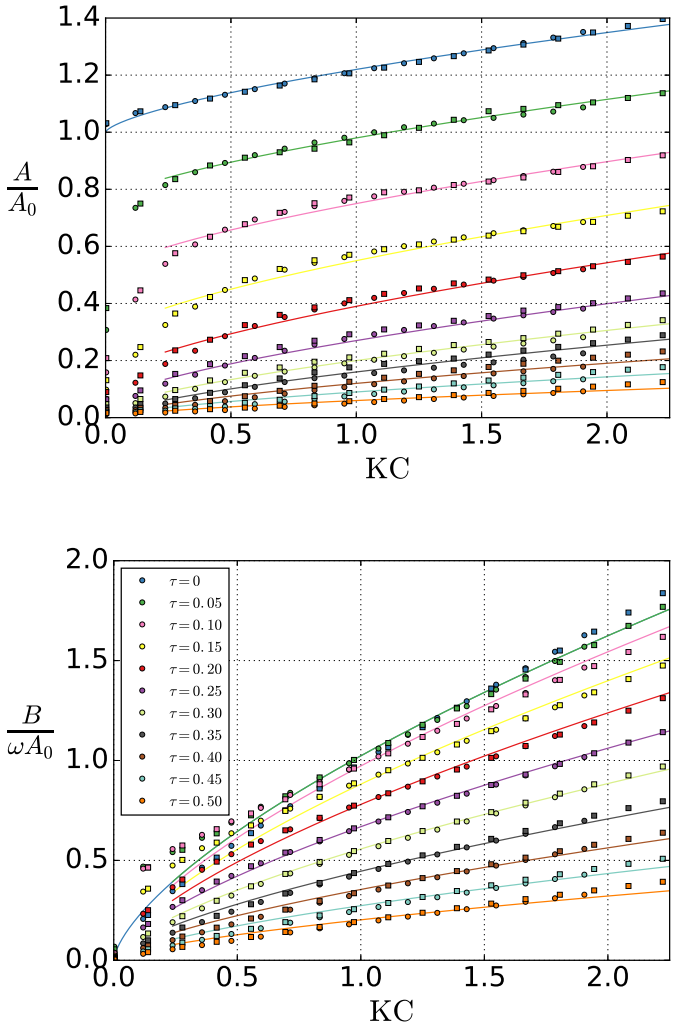

FIGURE 10. ADDED MASS (TOP) AND DAMPING (BOTTOM) COEFFICIENTS BASED ON CURVE-FIT OF CFD RESULTS TO EQS. (6) AND (7). CURVE-FIT COEFFICIENTS PRESENTED IN TABLE 5. CIRCULAR MARKERS: MODEL I. SQUARE MARKERS: MODEL II.

cular cylinders. In [3], a comparison was made between their results and experiments of a perforated plate with sharp openings. The perforation ratios were similar in the two cases. The protection structure yielded, in general, smaller added mass and damping coefficients than the perforated plate with sharp openings. Reynolds number effects must also be considered in cases of blunt members.

Compared to the results from the semi-analytical method by Molin, the presently proposed curve-fits yield in general smaller mean relative differences and are considerably better correlated

TABLE 5. COEFFICIENTS IN EQS. (6) AND (7) WHEN CURVE-FITTED TO THE CFD RESULTS. MEAN RELATIVE DIFFERENCE ($\overline{d_r}$) AND CORRELATION COEFFICIENT (r) BETWEEN CURVE-FIT AND CFD RESULTS.

τ	a_0	a_1	b_1	$\overline{d_r}$	r
0.00	1.000	0.216	10.1	3 %	1.00
0.05	0.748	0.230	10.1	2 %	1.00
0.10	0.498	0.252	9.58	4 %	0.99
0.15	0.281	0.271	8.72	5 %	0.99
0.20	0.132	0.261	7.67	4 %	0.99
0.25	0.055	0.222	6.57	2 %	1.00
0.30	0.017	0.181	5.48	4 %	0.99
0.35	0.000	0.156	4.44	7 %	0.99
0.40	0.000	0.120	3.49	11 %	0.99
0.45	0.000	0.087	2.69	15 %	0.99
0.50	0.000	0.057	2.04	16 %	0.99

with the CFD results. Compared to the RP by DNV GL, a strength of the proposed method is that an estimate for both the added mass *and* damping coefficients of perforated plates is easily obtained.

The curve fits for the perforated plates are based on results for both plate models I and II for $0.24 \leq \text{KC} \leq 2.2$. The results from the smallest KC numbers are ignored when performing the curve fitting for the perforated plates, as this gave a more realistic overall behavior of the curves. The number of holes on the plate is the important parameter for the added mass in the low KC limit. If a value for the added mass in the low-KC limit is needed, i.e. for $\text{KC} < 0.24$, one should use an alternative approach, e.g. a source method calculation.

CONCLUSION

Numerical results, in terms of hydrodynamic added mass and damping coefficients, from simulations of perforated plates in oscillating flow, were presented. Ten perforation ratios, τ, from 0.05 to 0.50, in addition to a corresponding solid plate, were investigated for $0.002 \leq \text{KC} \leq 2.2$. The results from the solid plate simulations were in good agreement with the analytical investigations by Graham [8], supporting the validity of the simulations. Our perforated plate CFD results were validated against previous experimental studies. Both the added mass and damping coefficients in general decrease with increasing perforation ratio. The decrease in added mass was largest, such that the

relative damping contribution on the total hydrodynamic force increased with increasing perforation ratio. All plates with perforation ratios greater than or equal to $\tau = 0.1$ were found to be damping dominant. The plates with $\tau < 0.1$ were added mass dominated for the small KC numbers, and dominated by damping for the larger KC numbers.

In addition to the numerical simulations, 3600 calculations were performed with Molin's semi-analytical method for estimating hydrodynamic coefficients of perforated plates. Considerable differences were found between the present CFD and Molin's method. Challenges with choosing the empirical coefficients in the semi-analytical method, μ and α, were highlighted, as also noted in recent literature.

Based on the relations for hydrodynamic coefficients from the analytical solid plate model by Graham, we presented a new semi-analytical method based on curve-fitting of our CFD results for perforated plates. The new model provide estimates of the added mass and damping as functions of the perforation ratio and amplitude of motion. Due to their simplicity, these relations can be a useful tool for estimating hydrodynamic coefficients of perforated plates. Further validation for more perforation ratios, as well as different types of perforated structures, would be favorable.

ACKNOWLEDGEMENT

The authors would like to thank Prof. Bernard Molin for his contributions to the present study. This work was financed by the Research Council of Norway, NFR project 237929 CRI MOVE.

REFERENCES

[1] Molin, B., 2011. "Hydrodynamic modeling of perforated structures". *Applied Ocean Research,* ***33***(1), pp. 1–11.

[2] Mentzoni, F., and Kristiansen, T., 2019. "Numerical modeling of perforated plates in oscillating flow". *Applied Ocean Research,* ***84***, pp. 1 – 11.

[3] Mentzoni, F., Abrahamsen-Prsic, M., and Kristiansen, T., 2018. "Hydrodynamic coefficients of simplified subsea structures". In Proceedings of the International Conference on Offshore Mechanics and Arctic Engineering.

[4] An, S., and Faltinsen, O. M., 2013. "An experimental and numerical study of heave added mass and damping of horizontally submerged and perforated rectangular plates". *Journal of Fluids and Structures,* ***39***(Supplement C), pp. 87–101.

[5] Sandvik, P. C., Solaas, F., and Nielsen, F. G., 2006. "Hydrodynamic forces on ventilated structures". In Proceedings of the International Offshore and Polar Engineering Conference, pp. 54–58.

[6] Molin, B., Remy, F., and Rippol, T., 2007. "Experimental study of the heave added mass and damping of solid and perforated disks close to the free surface". In Maritime Industry, Ocean Engineering and Coastal Resources - Proceedings of the 12th International Congress of the International Maritime Association of the Mediterranean, IMAM 2007, Vol. 2, pp. 879–887.

[7] Li, J., Liu, S., Zhao, M., and Teng, B., 2013. "Experimental investigation of the hydrodynamic characteristics of heave plates using forced oscillation". *Ocean Engineering,* ***66***, pp. 82 – 91.

[8] Graham, J. M. R., 1980. "The forces on sharp-edged cylinders in oscillatory flow at low Keulegan–Carpenter numbers". *Journal of Fluid Mechanics,* ***97***(2), pp. 331–346.

[9] Molin, B., 1989. "On the added mass and damping of porous or slotted cylinders". In Proc. 4th int. workshop water waves & floating bodies.

[10] Molin, B., 2001. "On the added mass and damping of periodic arrays of fully or partially porous disks". *Journal of Fluids and Structures,* ***15***(2), pp. 275 – 290.

[11] DNV GL AS. Modelling and analysis of marine operations. DNVGL-RP-N103 Edition July 2017. Obtained 2017-09-14.

[12] Chorin, A. J., 1968. "Numerical solution of the navier-stokes equations". *Mathematics of Computation,* ***22***(104), pp. 745–762.

[13] Singh, S., 1979. "Forces on bodies in an oscillatory flow". PhD thesis, Department of aeronautics, Imperial College, University of London.

[14] An, S., and Faltinsen, O. M., 2012. "Linear free-surface effects on a horizontally submerged and perforated 2d thin plate in finite and infinite water depths". *Applied Ocean Research,* ***37***, pp. 220 – 234.

[15] Molin, B., and Nielsen, F., 2004. "Heave added mass and damping of a perforated disk below the free surface". In Proceedings of the 19th International Workshop on Water Waves and Floating Bodies, Cortona, Italy.

[16] Blevins, R., 2003. *Applied Fluid Dynamics Handbook*. Krieger Pub.